Journal of Fluids and Structures (1998) **12,** 779–798
Article No. fl980164

LOCK-ON OF VORTEX SHEDDING DUE TO ROTATIONAL OSCILLATIONS OF A FLAT PLATE IN A UNIFORM STREAM

J. M. Chen and Y.-C. Fang

Department of Mechanical Engineering, National Chung Hsing University, Taichung, Taiwan

(Received 20 June 1997 and in revised form 20 April 1998)

The lock-on of vortex shedding induced by rotational oscillations of a flat plate normal to a uniform stream in its neutral position has been studied experimentally for Reynolds numbers in the range Re = 3000–8000. The onset of lock-on, which depends on the combination of the frequency and amplitude of the forcing, is examined by using spectral analysis of the wake velocity. The forcing frequency is set to a fixed value, between 80 and 120% of the natural shedding frequency of the stationary normal flat plate, while the angular forcing amplitude is varied to search for the lock-on regime. The lock-on regime is found to become narrower with increasing free-stream velocity. Effects of blockage on the lock-on regime are also investigated in some detail. For vortex locking-on to the frequency of the forcing above or below the natural shedding frequency, significant differences are observed in the distributions of fluctuating and time-mean base pressures. Flow visualization suggests that these differences are primarily due to the formation of shed vortices.

1. INTRODUCTION

It is well recognized that vortex streets are formed in the wake of bluff bodies over a wide range of Reynolds numbers. The organized and periodic shedding of vortices may result in considerable fluctuating loading on the body. When the shedding frequency is close to one of the characteristic frequencies of the body, resonant oscillations of the body can be excited, causing damaging instabilities. On the other hand, when the body is periodically oscillated by external forcing, the shedding frequency may be modified or shifted from its natural shedding frequency to the forcing frequency. This "lock-on" of vortex shedding to the forcing frequency provides potential means for active control of the wake flow behind a bluff body, and has numerous practical engineering applications. These applications include the areas of offshore exploration and drilling, civil and wind engineering, electric power transmission, heat transfer, and combustion.

Most of the studies on vortex lock-on have so far been restricted to flow past bluff bodies with simple geometry such as cylinders and flat plates. Early research on vortex shedding from forced-oscillating bluff cylinders has shown that lock-on can take place when the cylinder is undergoing either in-line oscillations with the incident flow or cross-flow oscillations. One of the most prominent characteristics of vortex lock-on is the bound of the lock-on regime, that is the combination of the frequency and amplitude of the forcing causing the onset of lock-on. The lock-on phenomena usually occur near the natural shedding frequency of the cylinder for cross-flow oscillations and near twice the natural shedding frequency for in-line oscillations. The lock-on frequencies for in-line oscillations of a circular cylinder were observed between 1·20 and 2·50 times the natural shedding frequency (Griffin & Ramberg 1976). The lock-on regime for cross-flow oscillations of

0889–9746/98/060779 + 20 $30.00

a circular cylinder is relatively reduced, and occurs between 0·7 and 1·25 times the natural shedding frequency (Koopmann 1967). Recent studies of Tokomaru and Dimotakis (1991) and Filler *et al.* (1991) have shown that lock-on can also be induced when the cylinder is subjected to rotational oscillations near the natural shedding frequency. However, the range of lock-on frequencies for rotational oscillations observed seems to be much smaller as compared with those in the two other oscillation modes. Body configuration also plays an important role in lock-on behaviour. Armstrong *et al.* (1986) observed that the lock-on regime of circular cylinders undergoing in-line oscillations, with free separation points, is approximately twice the breadth of D-section cylinders and flat plates, with fixed separation points. An overview of the flow characteristics of vortex shedding lock-on resulting from oscillations of bluff cylinders can be found in the paper of Griffin & Hall (1991). A wide range of vortex patterns induced by in-line and cross-flow oscillations of cylinders were phenomenologically described by Öngören & Rockwell (1988*a*, *b*). Most recently, numerical studies of Minewitsch *et al.* (1994), Sung *et al.* (1994) and Pan *et al.* (1995) also explored many details of the vortex lock-on phenomena. In particular, the use of pulsating monopole sources to induce the lock-on of vortex shedding from a circular cylinder by Pan *et al.* demonstrated an increase in the time-mean drag coefficient with increasing forcing frequency in the lock-on range. A similar trend was also observed experimentally by Nakamura & Hirata (1991) for transversely oscillating rectangular cylinders with the long side normal to the flow, that was an increase in the absolute base pressure coefficient with increasing reduced velocity in the lock-on range.

The aforementioned studies have generally led to a fairly consistent picture of the lock-on regime depending on oscillation modes and body configurations. However, the effects of Reynolds number on lock-on regime are yet to be fully understood. Griffin & Hall (1991) in their review paper compared (i) the bounds of the lock-on regime measured by several authors for circular cylinders due to in-line oscillations and (ii) flow perturbations for Reynolds numbers in the range 80–40 000. They found good agreement between the limits of the lock-on regime for the two types of external forcing means. They also pointed out that Reynolds number effects on the bounds of lock-on regime are relatively small. However, for cross-flow oscillations, the bounds of the lock-on regime measured by Koopmann (1967) seem to depend upon Reynolds number in the range 100–300. In a similar experiment, Stansby (1976) also found different bounds of lock-on regime between Reynolds numbers of 3600 and 9200.

In comparison with vortex lock-on occurring around bluff cylinders, there are very few reported studies of lock-on phenomena for flow around an oscillating flat plate. The existence of vortex lock-on for a stationary normal flat plate immersed in a stream containing a pulsating component was examined experimentally by Armstrong *et al.* (1986) and numerically by Sung *et al.* (1994). The flow past a rotationally oscillating flat plate was investigated experimentally by Kelso *et al.* (1993) and Chua *et al.* (1990), but neither of them reported lock-on phenomena. Nevertheless, rotational oscillations serve as a potentially exciting system for the active control of vortex formation in bluff body flows (Griffin and Hall 1991).

The present experimental study aims to reveal the fundamental characteristics of vortex lock-on due to rotational oscillation of a flat plate which is normal to a uniform stream in its neutral position. The route leading to the lock-on state as well as the bounds of lock-on regime were examined by the use of velocity spectra measured in the wake of the oscillating plate. The width of the test plate and the velocity of the uniform stream were parametrically varied in the experiments. These variations allow us to investigate the effects on lock-on phenomena due to Reynolds number and blockage in detail. Measurements of fluctuating and mean pressures on the plate surfaces incorporated with smoke-wire visualization of the

vortex formation were carried out to explore the response of the plate to vortex shedding, particularly for the cases where lock-on occurred.

2. EXPERIMENTAL SET-UP

The experiments were performed in a low-speed open-type wind tunnel with a square test-section of 305 mm × 305 mm and 1100 mm in length. The flow into the test–section had turbulence levels less than 0·5% for the velocity range tested in the experiments. Figure 1 shows the flow configuration of the present investigation. The measurements were carried out using flat plates of 6 mm thickness and 303 mm span. Each of the plates was bevelled at 45° on its top and bottom edges, from which the flow was expected to fully separate. The plates were constructed from Plexiglas and were milled and polished. A total of six flat plate models with width $H = 30$, 40, 45, 50, 60 and 80 mm were tested for the present investigation. The plate model was mounted spanwise across the test-section and vertically oriented in its neutral position. The gap between the plate and the side-walls was 1 mm at each side. For the dynamic tests, the model was oscillated sinusoidally about its mid-chord ($y/H = 0$) by a servomotor. The servomotor was controlled by a personal computer with a feedback loop to ensure a sinusoidal waveform of the oscillation. An optical encoder coupled to the motor shaft was able to signify the transient angle of incidence of the model to an accuracy of 0·09°. An actual time history of the oscillation schedule is shown in Figure 2 which exhibits a well-defined sinusoidal waveform. Accuracy of the oscillation frequency and amplitude is critical to the determination of the onset of lock-on. Repeat tests showed that the uncertainty of oscillation frequency and amplitude were no more than $\pm$ 0·01 Hz and $\pm$ 0·1°, respectively.

The velocity of flow behind the test plate was measured by a constant-temperature anemometer (TSI IFA 100) in conjunction with a hot-wire probe. The velocity signal was processed by a spectrum analyzer (HP 3582) which was able to display the response in both the time and frequency domains. The measurements were carried out for free-stream velocity U in the range 1·05–2·5 m/s, and Reynolds number $\mathrm{Re} = UH/\nu$ in the range 3000–8000, where ν is the kinematic viscosity. During each measurement of vortex shedding frequency, the probe was placed in the centreplane of the test-section at a downstream station of $x/H = 3{\cdot}5$. The transverse position of the probe was set at a distance $y/H \approx 2$

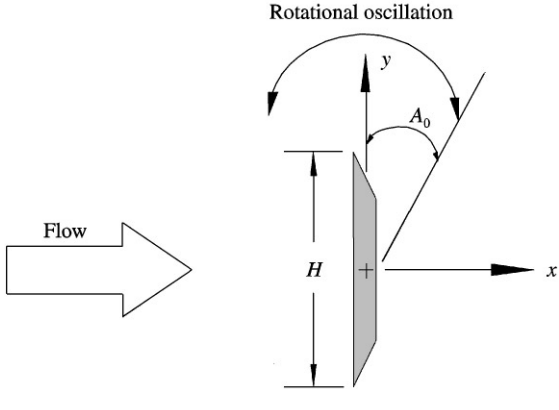

Figure 1. Cross-section of the rotationally oscillating flat plate with its neutral position normal to the free stream.

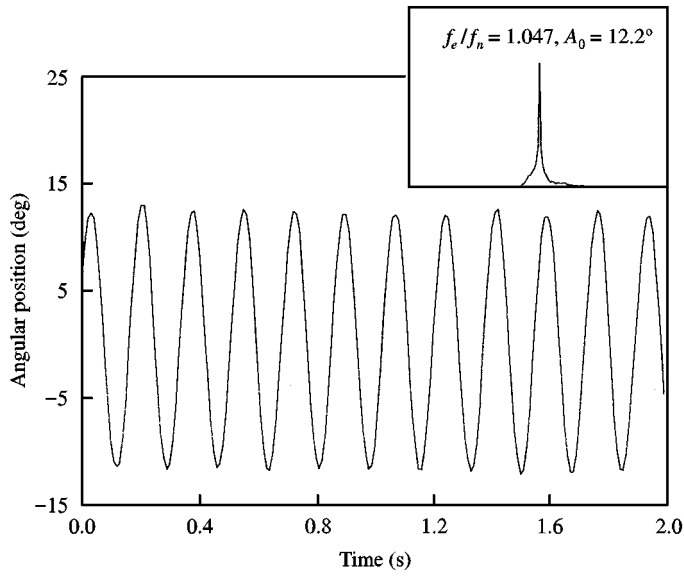

Figure 2. Actual time history of oscillation schedule and the corresponding spectrum.

from the centreline of the wake in order to preclude interference in the recorded velocity signal from vortices of opposing sign (Griffin & Ramberg 1976). The mean spectra were averaged over at least ten individual spectra, showing the uncertainty of the shedding frequency presented to be less than 0·5%.

For measurements of surface pressures, 12 pressure ports of 0·75 mm in diameter were instrumented along the mid-span of the test plate ($H = 45$ mm). Half of the pressure ports were located on the front face at unequal spacing. The remaining half of the pressure ports were located on the rear face. To obtain a finer spatial resolution for pressure distributions along the plate, measurements were also made with the upper edge of the plate down. Fluctuating and time-averaged pressures were measured using Setra 239 differential pressure transducers of range 6·35 mm of water. The transducers were connected to the pressure ports with short tubes of equal length and in reference to the free-stream wall pressure at $2H$ upstream of the test plate. The frequency response of the pressure transducer itself was higher than 2·0 kHz. Although the connection of the tubing to the transducer could reduce the dynamic response, such an arrangement for pressure measurements suffices for the present investigation. The pressure signal was recorded by a multi-channel analog data acquisition memory (ADAM ADC0512) which had an individual A/D converter on each channel. The estimated uncertainty (due to random errors) of the mean pressure coefficient C_p was approximately within $\pm$ 0·005.

To supplement the pressure measurements, the smoke-wire technique was employed to visualize the flow field. A corrugated nichrome wire of 100 μm diameter was placed vertically in the centreplane of the test-section. To generate smoke streaks the wire was heated at a voltage of 20–30 V. The visualized flow field was illuminated by an argon laser light sheet and recorded by a frame grabber (Coreco Oculus-F/64) with a CCD camera. Photographs of the flow image was taken from a film recorder. The flow visualization and pressure measurements were performed at the same free-stream velocity $U = 1{\cdot}5$ m/s.

3. RESULTS AND DISCUSSION

3.1. Route to Vortex Lock-on

The commonly termed vortex shedding lock-on occurs when the natural shedding frequency of a bluff body disappears in favour of the forcing frequency of the disturbances (Blevins 1990). The lock-on state is accompanied by a strong interaction between the natural vortex shedding and the forced body oscillation. The occurrence of lock-on depends on the combination of the frequency and amplitude of the forced body oscillations. Experimentally, various techniques have been employed by different investigators to examine the onset of lock-on. For the present experiments, the onset of lock-on was determined by the use of a real-time spectrum analyzer with a hot-wire probe placed in the wake of the test plate for acquiring the vortex-induced fluctuating velocity signal. At a constant free-stream velocity, the natural vortex-shedding frequency, f_n, was first obtained for the stationary normal flat plate. Then the plate was forced to oscillate at a fixed frequency f_e, in the range $0{\cdot}8 \leq f_e/f_n \leq 1{\cdot}2$. As the oscillation amplitude of the plate was slowly increased, a certain threshold amplitude was reached. At this threshold amplitude, the vortex-shedding frequencies were replaced by a single sharp spike on the spectrum with its value identical to the frequency of forced oscillation, and thereafter this state persisted. The route leading to the occurrence of lock-on is explained in the following paragraphs for the plate of $H = 45$ mm rotationally oscillated at $U = 1{\cdot}5$ m/s. The blockage ratio of the test plate was 14·7%. The effects of blockage will be discussed later.

Figure 3 shows the amplitude spectrum of the wake velocity measured for the stationary normal plate. The natural shedding frequency of the unforced plate is found at $f_n = 5{\cdot}52$ Hz with a broad-band peak. The broad-band peak is possibly connected with three-dimensional effects as indicated by Chua *et al.* (1990). To achieve the state of lock-on, the forced oscillation frequency can be approached either from the lower-frequency limit $f_e < f_n$ or from the higher-frequency limit $f_e > f_n$. Figure 4 shows the amplitude spectra of the wake velocity for an approach of higher frequency limit at $f_e/f_n = 1{\cdot}047$. At a small forcing amplitude $A_0 = 2{\cdot}0^\circ$, the plate oscillation is superimposed upon the wake flow resulting in the appearance of f_e in the velocity spectrum in addition to the vortex-shedding frequency f_v, which is not necessarily the same as the natural shedding frequency of the unforced plate. As the forcing amplitude is increased to $A_0 = 4{\cdot}5^\circ$, the spectrum has two peaks of nearly the same importance. Apparently, the frequency band of f_v becomes broader while the peak of f_e remains sharp. In fact, it was observed on the real-time spectrum analyzer that f_v was

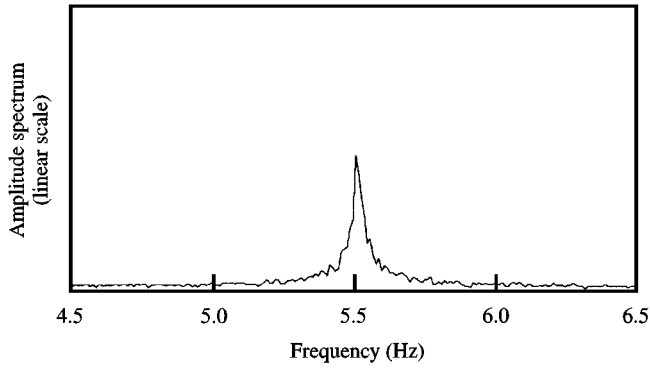

Figure 3. Amplitude spectrum of the wake velocity for the stationary normal flat plate.

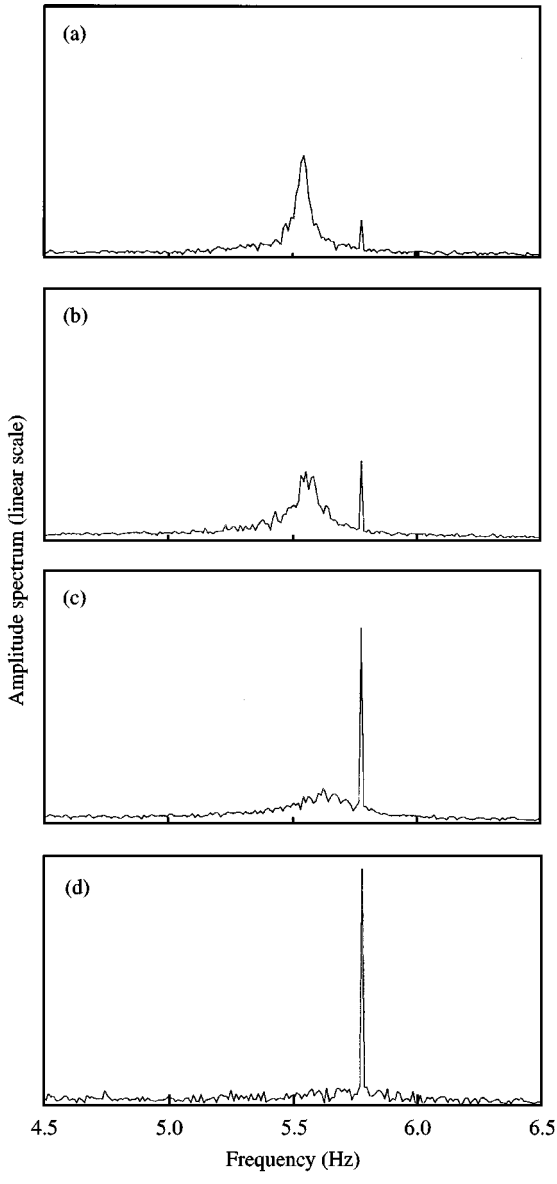

Figure 4. Amplitude spectrum of the wake velocity for an approach to lock-on at $f_e/f_n = 1{\cdot}047$ for: (a) $A_0 = 2{\cdot}0^\circ$; (b) $A_0 = 4{\cdot}5^\circ$; (c) $A_0 = 9{\cdot}0^\circ$; (d) $A_0 = 12{\cdot}2^\circ$.

shifting within the frequency band, rather than staying at a fixed value like f_e. With an increase in forcing amplitude to $A_0 = 9{\cdot}0^\circ$, the peak amplitude of f_v is further reduced. Meanwhile, the peak amplitude of f_e is relatively much enlarged, signifying energy conveyance from f_v to f_e. At $A_0 = 12{\cdot}2^\circ$, only a single dominant, sharp peak f_e appears in the spectrum, representing the state of lock-on. During the state of lock-on, the vortex shedding is synchronized to the forced oscillation of the plate. Figure 5 demonstrates the variation of the frequency ratio f_v/f_e with forcing amplitude for the higher-frequency-limit approach. The transition to lock-on occurs in the following manner: the frequency ratio gradually

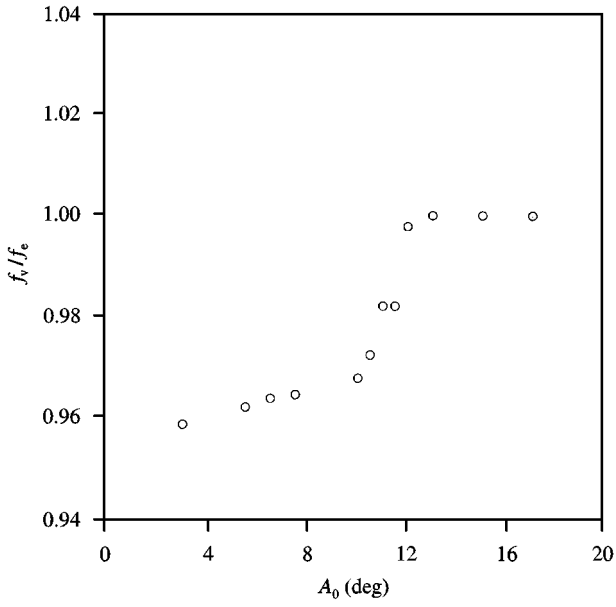

Figure 5. Variation of frequency ratio f_v/f_e with forcing amplitude for an approach to lock-on at $f_e/f_n = 1{\cdot}047$.

increases with increasing forcing amplitude, and then it rises sharply to reach a flat ratio of unity, at which point lock-on occurs.

Figure 6 shows the spectra of the wake velocity for an approach to lock-on at a lower frequency limit, $f_e/f_n = 0{\cdot}967$. The onset of lock-on occurs at $A_0 = 12{\cdot}0^\circ$. With an increase in the forcing frequency, the spectra show that the peak amplitude of f_v is gradually depressed while the amplitude of f_e becomes larger, similarly to the trend observed in Figure 4 for the approach to the higher-frequency limit. However, the vortex-shedding frequency f_v observed in Figure 6 seems to remain unchanged as the plate is oscillated below the onset forcing amplitude ($A_0 < 12{\cdot}0^\circ$), unlike the case of higher-frequency-limit approach.

3.2. Limits of Lock-on Regime

Figure 7 shows the limits of lock-on regime for the plate of $H = 45$ mm at $U = 1{\cdot}5$ m/s. The forcing amplitude A_0 of the oscillating plate is plotted against the Strouhal number ratio $\mathrm{St}_e/\mathrm{St}_n$, where $\mathrm{St}_e = f_e H/U$ is the forced Strouhal number, and $\mathrm{St}_n = f_n H/U$ is the Strouhal number of the unforced plate. The data points are least-squares fitted with second-order polynomials. Both the upper- and lower-frequency limits are similar functions of the forcing amplitude. Apparently, lock-on can be forced to occur with the smallest forcing amplitude ($A_0 = 2{\cdot}0^\circ$) at the natural shedding frequency f_n, indicating a replacement of the broad-band peak for the unforced plate by a dominant, sharp peak for oscillation of the plate at a very small amplitude. With an increase of the difference between f_e and f_n in either the positive or negative direction, the forcing amplitude required for lock-on tends to increase. In comparison with an oscillating circular cylinder (Griffin & Hall 1991; Armstrong *et al.* 1986), with free separation points, the normal flat plate with fixed separation points has a narrower lock-on region. This difference in the character of lock-on for the two types of bluff bodies was also addressed by Bearman (1984) and Armstrong *et al.* (1986).

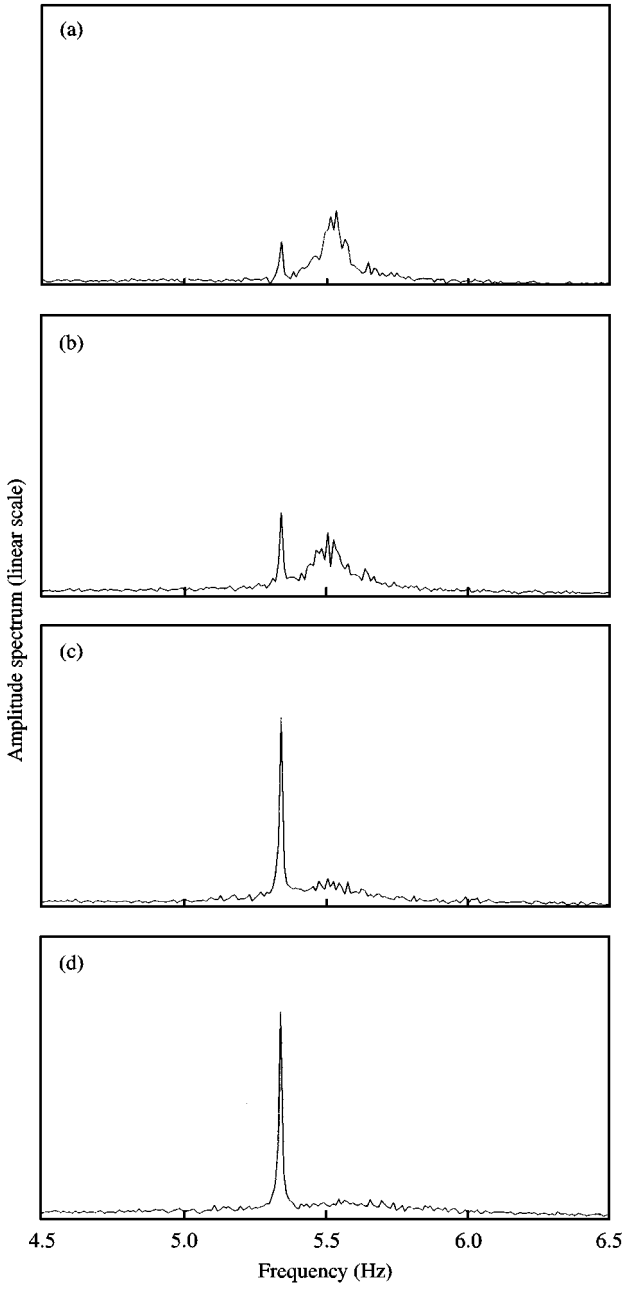

Figure 6. Amplitude spectrum of wake velocity for an approach to lock-on at $f_e/f_n = 0{\cdot}967$ for: (a) $A_0 = 2{\cdot}0^\circ$; (b) $A_0 = 4{\cdot}5^\circ$; (c) $A_0 = 9{\cdot}0^\circ$; (d) $A_0 = 12{\cdot}0^\circ$.

In order to investigate the influence of Reynolds number on the limit of the lock-on regime, plates of different width ($H = 30$–80 mm) were tested at free-stream velocity in the range $U = 1{\cdot}05$–$2{\cdot}5$ m/s. It has been known that the Strouhal number of a stationary normal flat plate maintains a nearly constant value for a wide range of Reynolds numbers (Novak 1973). This is true for changes in Reynolds numbers by varying the plate width as

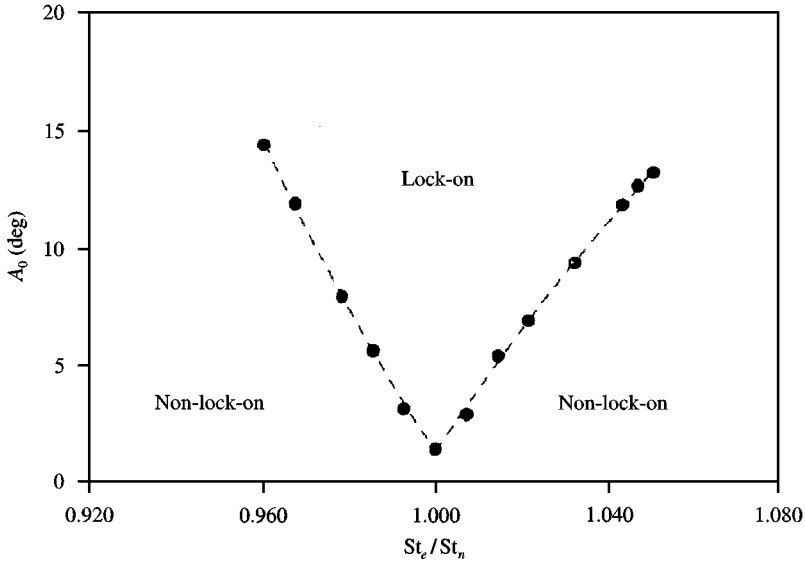

Figure 7. Limits of the lock-on regime for the plate with $H = 45$ mm at $U = 1{\cdot}5$ m/s.

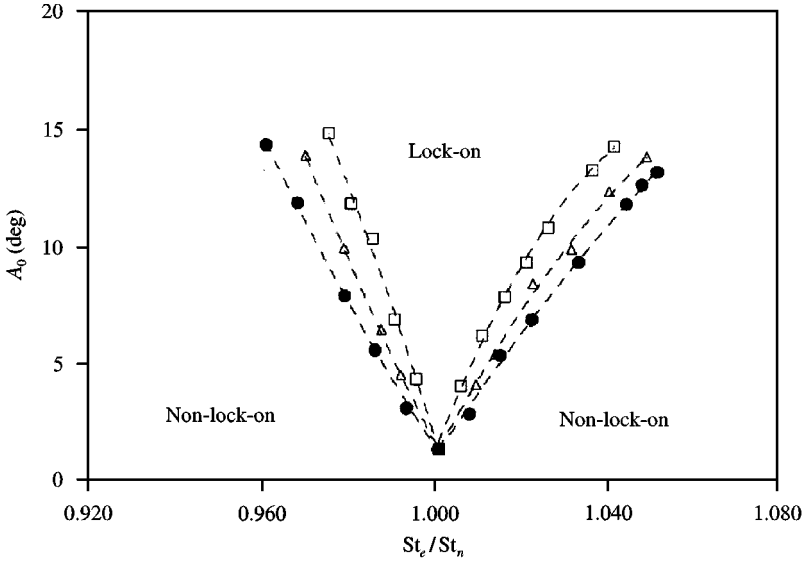

Figure 8. Limits of the lock-on regime for different plates at the same free-stream velocity $U = 1{\cdot}5$ m/s: ●, $H = 45$ mm; △, $H = 60$ mm; □, $H = 80$ mm.

well as the free-stream velocity (Chen & Fang 1996). These findings suggest that the vortex-shedding frequency of an oscillating normal flat plate may vary with H and U as well. Effects on the limits of the lock-on regime with respect to the variations of plate width and free-stream velocity are discussed in what follows.

Figure 8 shows the limits of lock-on regime for $H = 45$, 60 and 80 mm at the same free-stream velocity $U = 1{\cdot}5$ m/s. It appears that the lock-on regime becomes narrower with an increase of the plate width. In other words, at the same Strouhal number ratio St_e/St_n,

the onset forcing amplitude is larger for a wider plate. However, the dependence of the lock-on regime on plate width observed in Figure 8 disregards the blockage effects of the plate. The blockage ratios were 0·147, 0·197 and 0·262 for the plates with $H = 45$, 60 and 80 mm, respectively. There are two major effects on a bluff body due to the wind tunnel walls, namely, the confinement effect and the displacement effect (Ota *et al.* 1994). The confinement effect results in an increase of local velocity, while the displacement effect caused by boundary layers developing on the walls may be neglected for the present experiments which were performed at relatively high Reynolds numbers. In order to account for the effects of blockage, Chen & Fang (1996) used a semi-empirical formula originally proposed by Ota *et al.* (1994) for the correction of the Strouhal number.

$$\mathrm{St} = \mathrm{St}_o/(1 - \xi K), \tag{1}$$

where St_o is the corrected Strouhal number representing the Strouhal number in an unbounded flow, ξ is the correction factor for blockage, and K is the blockage ratio. For a stationary normal flat plate, St_o and ξ were approximated to be 0·136 and 1·21, respectively, for blockage ratios $K = 0{\cdot}043$–$0{\cdot}262$ (Chen & Fang 1996). Equation (1) is in fact used for the correction of the local velocity, i.e., the free-stream velocity U is divided by $(1 - \xi K)$ to obtain the corrected velocity U_m,

$$U_m = U/(1 - \xi K). \tag{2}$$

Figure 9(a) shows the lock-on limits for different plates at the same corrected velocity $U_m = 1{\cdot}83$ m/s. It is observed that the lock-on limits for the three plates fall close to the same curve of second-order polynomials. Similar results are also found for a higher corrected velocity $U_m = 2{\cdot}57$ m/s, as depicted in Figure 9(b). Note that the lock-on regime measured at $U_m = 2{\cdot}57$ m/s is smaller than that measured at $U_m = 1{\cdot}83$ m/s. The observations of Figure 9 suggest that the limits of the lock-on regime are insensitive to the plate width for forced rotational oscillation in an unbounded free stream.

Changes in Reynolds number can also be made by varying free-stream velocity. The lock-on limits for the plate of $H = 45$ mm at four different free-stream velocities are presented in Figure 10. It is found that an increase in velocity results in a narrower regime of lock-on. In other words, the occurrence of lock-on for higher velocity at the same $\mathrm{St}_o/\mathrm{St}_n$ needs larger oscillation amplitude.

The results of Figures 9 and 10 lead one to conclude that the lock-on regime for a flat plate undergoing rotational oscillations can be influenced by the change of velocity rather than by the change of plate width. These results are consistent with the observations by Stansby (1976) for transverse oscillations of a circular cylinder. In comparison with previous studies, the present experiments offer a more detailed investigation of parameter effects on the limits of the lock-on regime.

3.3. Pressure Measurements

Measurements of surface pressure were used to explore the response of the flat plate to vortex shedding under various oscillation conditions. The surface pressure data may also be used to explain the drag force acting on the plate for some cases. Prior to the measurements on the oscillating plates, pressures on the stationary normal plate were measured. In order to ascertain the accuracy of the pressure measurements as well as to account for the blockage effects, the drag coefficient for the unforced case is computed from the measured pressure distribution and compared with the data of previous studies. The separated flow

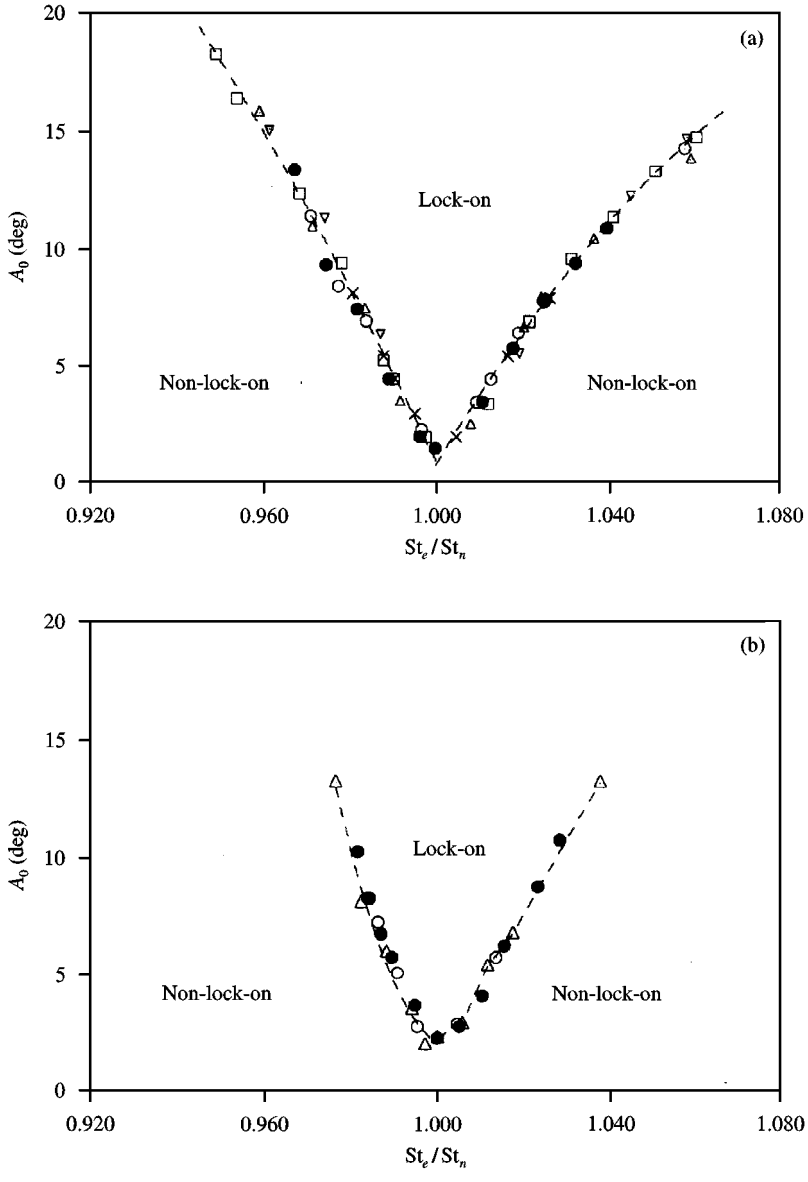

Figure 9. Limits of the lock-on regime for different plates at the same corrected velocity: ×, $H = 30$ mm; ○, $H = 40$ mm; ●, $H = 45$ mm; △, $H = 50$ mm; □, $H = 60$ mm; ▽, $H = 80$ mm. (a) $U_m = 1{\cdot}83$ m/s; (b) $U_m = 2{\cdot}57$ m/s.

past a two-dimensional flat plate may be modelled by the potential flow mapping scheme proposed by Parkinson and Jandali (1970). This mapping scheme can be used to compute the pressure distribution over the front face once the base pressure C_{pb} has been prescribed, i.e.

$$C_p(\theta) = 1 - \sin^2\theta/(\kappa - \cos\theta)^2, \tag{3}$$

where $\kappa = (1 - C_{pb})^{-1/2}$ and $y = 0{\cdot}5H\sin\theta$ is the distance from the axis. Favourable pressure distributions have been obtained by Parkinson & Jandali (1970) and Gaster &

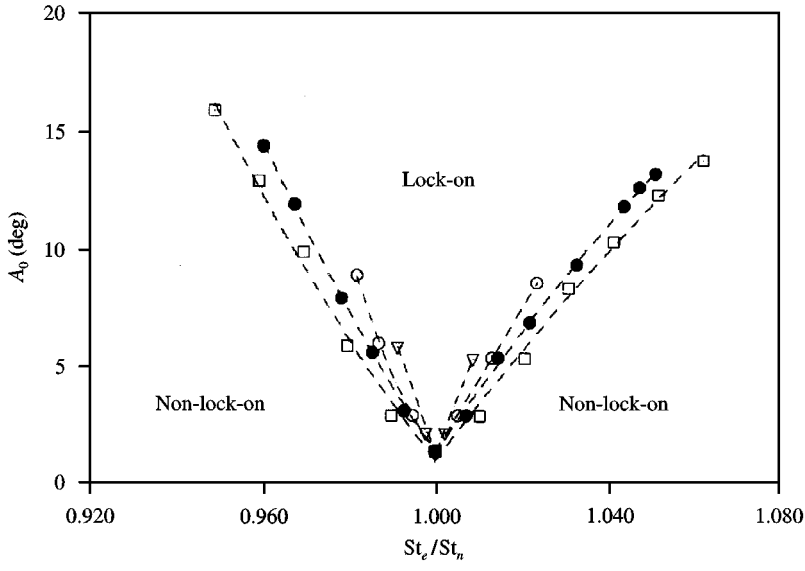

Figure 10. Limits of the lock-on regime for the plate of $H = 45$ mm at: □, $U = 1{\cdot}05$ m/s; ●, $U = 1{\cdot}50$ m/s; ○, $U = 2{\cdot}10$ m/s; ▽, $U = 2{\cdot}50$ m/s.

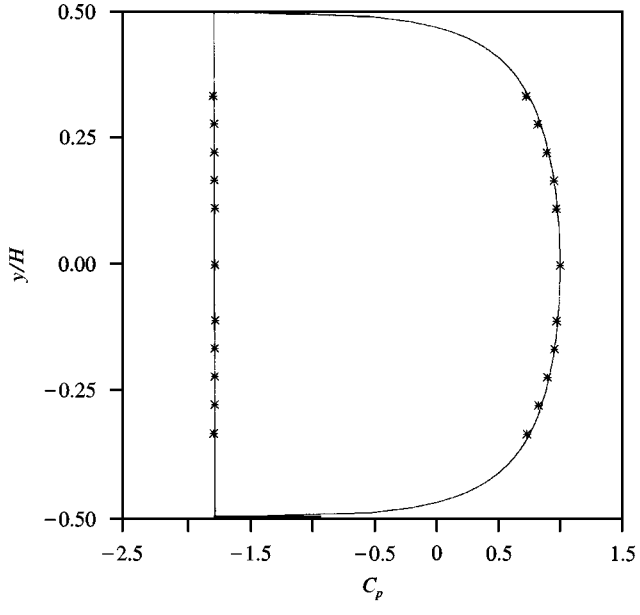

Figure 11. Comparison of the time-mean surface pressure coefficients measured for the plate of $H = 45$ mm with the distribution curve calculated from equation (3): ×, present data; ——, equation (3).

Ponsford (1984) in their corresponding cases. Figure 11 compares the time-mean surface pressure coefficients measured for the plate of $H = 45$ mm with the distribution curve calculated from equation (3). The measurements of C_p on the base exhibit a remarkably flat distribution at $C_{pb} = -1{\cdot}84$, and the experimental data of C_p on the front face agree well with the calculated curve. This agreement enables one to further compute the drag

coefficient, by integrating the pressure given by equation (3) over the plate surface, to be $C_D = 2{\cdot}57$, which is somewhat higher than the value of 2·13 measured by Fage and Johansen (1927) and 1·74 by Roshko (1955) in an essentially unbounded stream. This difference may be attributed to the blockage of the plate of $H = 45$ mm ($K = 14{\cdot}7\%$). Two formulas are used to correct the drag coefficient due to blockage effects. One is to correct the local flow velocity as proposed previously for Strouhal number,

$$C_D = C_{Do}/(1 - 1{\cdot}21\,K)^2, \tag{4}$$

where the uncorrected drag coefficient C_D is expressed using the corrected one C_{Do} in an unbounded flow, and the square term in the denominator relates to the correction of the local velocity appearing in the reference dynamic pressure $0.5\rho U^2$. The second is a semi-empirical correction formula suggested by Ota *et al.* (1994), in which C_{Do} and the correction factor for C_D can be obtained by the use of the least-square curve fitting as

$$C_D = C_{Do}/(1 - 2{\cdot}14\,K). \tag{5}$$

Both curves of equations (4) and (5) are presented in Figure 12 in comparison with the drag coefficients measured by Fage & Johansen (1927) and Roshko (1955) as well as the data of Awbi adopted from Ota *et al.* (1994). Good agreement is found for the comparison for blockage ratios less than 25%. This indicates that for the plate ($H = 45$ mm) employed for pressure measurements, the only significant effect of blockage is to produce an apparent increase in the local free-stream velocity. The comparison presented in Figure 12 also implies accurate pressure measurements of the present investigation.

Pressure measurements on a normal flat plate undergoing forced oscillations were also carried out using the plate of $H = 45$ mm. These measurements were made for three

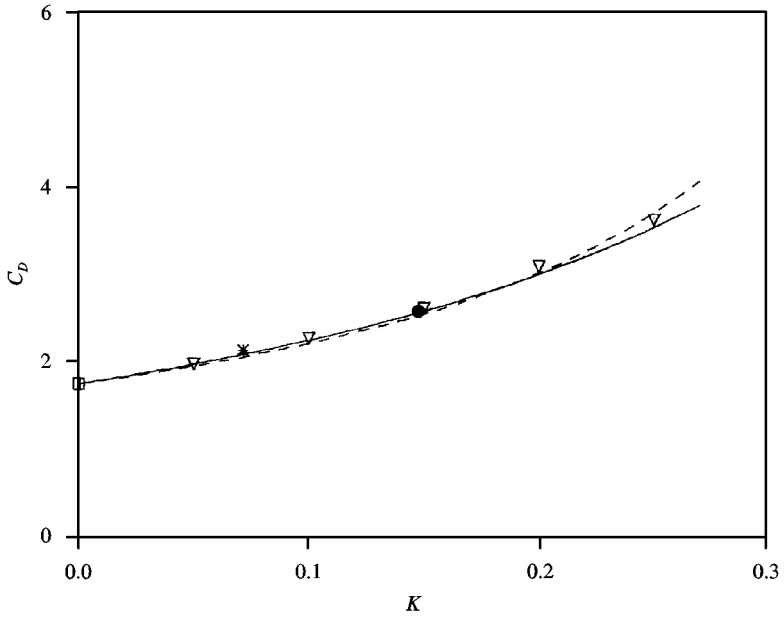

Figure 12. Comparison of the correction formula for C_D with experimental data: ●, present; ×, Fage & Johansen (1927); □, Roshko (1955); ▽, Awbi; ——, equation (4); – – –, equation (5).

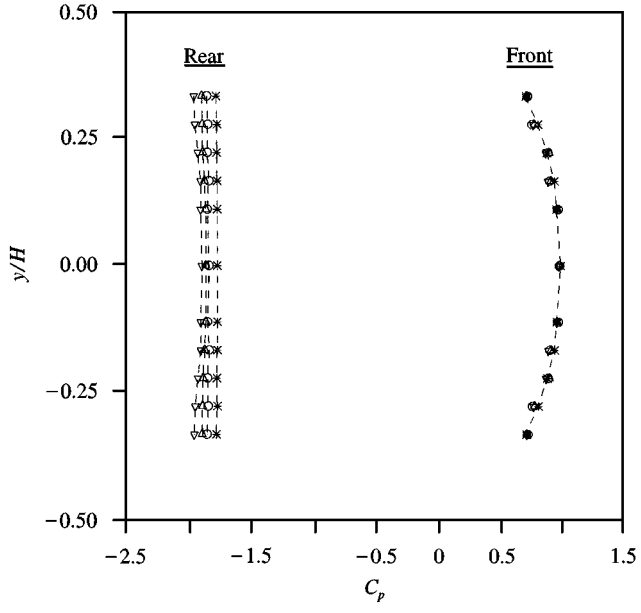

Figure 13. Pressure distributions on the front and rear faces at $f_e/f_n = 1{\cdot}000$ ($H = 45$ mm, $U = 1{\cdot}5$ m/s) for: ×, stationary; ○, $A_0 = 2{\cdot}0°$; △, $A_0 = 5{\cdot}5°$; ▽, $A_0 = 9{\cdot}0°$.

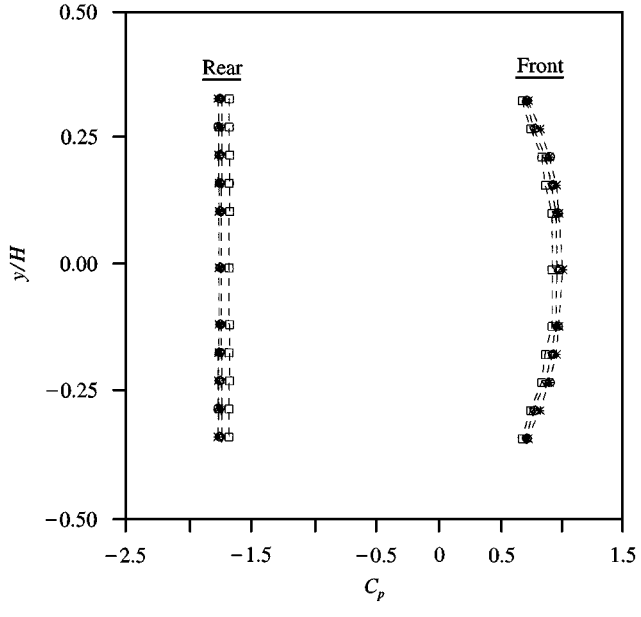

Figure 14. Pressure distributions on the front and rear faces at $f_e/f_n = 0{\cdot}967$ ($H = 45$ mm, $U = 1{\cdot}5$ m/s) for: ×, stationary; ○, $A_0 = 5{\cdot}5°$; △, $A_0 = 9{\cdot}0°$; ▽, $A_0 = 12{\cdot}0°$; □, $A_0 = 20{\cdot}0°$.

different forcing frequency regions, namely (i) at the Strouhal frequency $f_e/f_n = 1{\cdot}000$; (ii) the lower-frequency limit; (iii) the higher-frequency limit.

It has been shown in Figure 7 that the lock-on state can be induced with the least oscillation amplitude at the natural shedding frequency. Figure 13 shows the pressure

distributions on the front and rear faces of the plate locked-on at the natural shedding frequency for different oscillation amplitudes $A_0 = 2{\cdot}0$, 5·5 and 9·0°. As can be seen, the base pressure distributions are nearly uniform along the plate except for the case of $A_0 = 9{\cdot}0°$ in which the values of C_p appear to be slightly lower near the edges. The base pressure level is seen to become progressively more negative as the oscillation amplitude increases, while the front face pressure distribution seems to be unchanged, indicating an increase in C_D. It is worth noting that even at a small forcing amplitude, $A_0 = 2{\cdot}0°$, the magnitude of the lock-on base pressure level is found to be larger than that of the unforced case by an amount of 0·1 in C_p. Kelso *et al.* (1993) in an experimental study of a surface-mounted plate oscillating at small amplitude also found the base pressure level becoming more negative by 0·07 in C_p as compared with the unforced plate. They attributed this decrease in C_p to a reduction of the reattachment length for the oscillating plate. For the present experiment, however, the decrease of the base pressures may be due to the fact that forced oscillation in the lock-on region tends to encourage the flow to be more two-dimensional, with vortices rolling up more uniformly spanwise than in the unforced case (Chua *et al.* 1990). Moreover, at larger forcing amplitudes, the shed vortices are expected to be more organized, resulting in an increase in C_D.

Figure 14 shows the pressure distributions on the front and rear faces of the plate at a lower limit frequency, $f_e/f_n = 0{\cdot}967$, for oscillation amplitudes $A_0 = 5{\cdot}5$, 9·0, 12·0 and 20·0°. It has been shown earlier that the vortex shedding becomes locked-on at $A_o = 12.0°$. The pressure distributions on the front face for smaller amplitudes ($A_0 = 5{\cdot}5$ and 9·0°) are observed to nearly coincide with that on the unforced plate. At the lock-on amplitude $A_0 = 12{\cdot}0°$, the front pressure values appear to drop. The pressure value further decreases at $A_0 = 20{\cdot}0°$. The reasoning for the drop of front face pressure is speculated as follows. The flow at the front is a potential flow and this requires the stagnation point to be on the plate. However, during the rotational oscillation of the plate, the stagnation point is no longer fixed at the plate mid-chord ($y/H = 0$). Then the time-mean value of C_p at $y/H = 0$ may be equivalent to that which occurs on a stationary inclined flat plate, becoming smaller than unity (Yeung & Parkinson 1997). Correspondingly, with an increase in the oscillation amplitude, the time-mean front-face pressure is expected to decrease. In any event, more analytical and experimental work needs to be carried out to clarify this speculation. On the rear face, the pressure distributions appear to be flat for all forcing amplitudes. For the non-lock-on cases, the pressure levels are maintained at a nearly constant value. Once the shedding is locked-on at $A_0 = 12{\cdot}0°$, the base pressure is slightly increased by 0·04 in C_p. As the forcing amplitude is further increased to $A_0 = 20{\cdot}0°$, the increment of C_p is enlarged by 0.1. In comparison with the unforced plate, the drop of pressures on the front face and rise on the rear face signifies a decrease in C_D for the plate oscillating at the lower limit frequency and at amplitudes in the lock-on regime. The rise of rear face pressure level for lower-frequency-limit lock-on can be further explained by comparing the smoke-wire visualizations portrayed in Figures 15 and 16 for the unforced plate and the oscillating plate at $f_e/f_n = 0{\cdot}967$ and $A_0 = 20{\cdot}0°$, respectively. For each of the cases, two photographs are presented, one for vortex shed from the top edge and the other from the bottom edge. It is found that the separated shear layer right behind the plate is bent to form a larger curvature in roll-up for the lower-frequency-limit lock-on flow than that for the unforced flow. As a result, the suction pressure behind the lower-frequency-limit plate is less intensified by the shed vortices. Also note that in both cases the shed vortices develop to cover almost the entire rear face of the plate, causing flat pressure distributions on the rear face, as seen in Figures 11 and 14.

Figure 17 shows the pressure distributions on the front and rear faces of the plate oscillating at a higher limit frequency $f_e/f_n = 1{\cdot}047$ for non-lock-on and lock-on oscillation

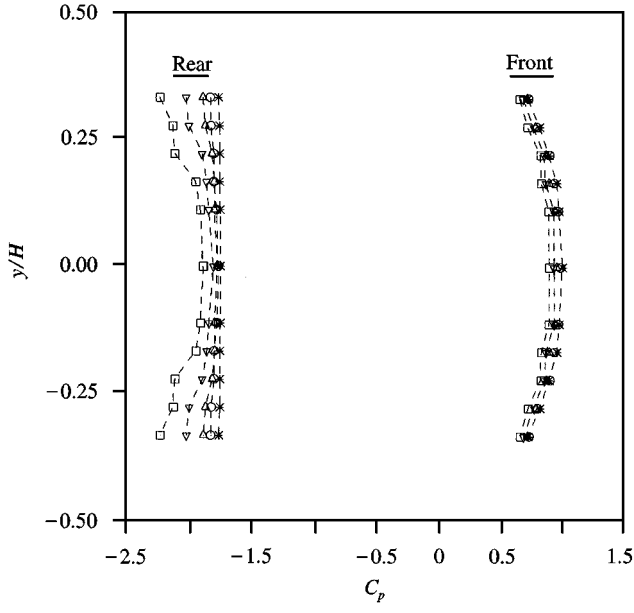

Figure 17. Pressure distributions on the front and rear faces at $f_e/f_n = 1{\cdot}047$ ($H = 45$ mm, $U = 1{\cdot}5$ m/s) for: ×, stationary; ○, $A_0 = 5{\cdot}5°$; △, $A_0 = 9{\cdot}0°$; ▽, $A_0 = 12{\cdot}2°$; □, $A_0 = 16{\cdot}0°$.

amplitudes $A_0 = 5{\cdot}5$, 9·0, 12·2 and 16·0°. The variation of the pressure distribution on the front face with oscillation amplitude shows the same trend as the one oscillating at a lower limit frequency (Figure 14). However, the pressure distributions on the rear face appear to be quite different from the uniform base pressure observed in the case of the lower frequency limit. At non-lock-on amplitudes, $A_0 = 5{\cdot}5$ and 9·0°, the mean base pressure has the same value as for the unforced plate at the middle of the plate but no longer maintains a constant value along the rear face, where it is lower near the edges. Moreover, the base pressures slightly shift in the negative sense with increasing amplitude of forcing. The falling off of base pressure near the edges, according to Chua *et al.* (1990), is a consequence of the shed vortices forming closer to the plate with an increase in forcing amplitude. Once lock-on is reached at $A_0 = 12{\cdot}2°$, it is observed that the base pressures become much more negative, particularly near the plate edges, indicating a significant rise in C_D. The decrease of base pressures is more appreciable at a larger lock-on amplitude, $A_0 = 16{\cdot}0°$. At this forcing amplitude, a low-pressure plateau region is seen to occur at the second and third pressure ports ($y/H = \pm 0{\cdot}28$ and $\pm 0{\cdot}21$, respectively) closest to the edges, near where the shed vortices develop. This is evidenced by the smoke-wire visualization of the flow as depicted in Figure 18 for the plate oscillating at $f_e/f_n = 1{\cdot}047$ and $A_0 = 16{\cdot}0°$. These pictures show that the separated shear layer rolls up with a larger curvature (smaller in diameter), to form a vortex much closer to the plate than those observed in the unforced and lower-frequency-limit cases.

In addition to the time-mean pressures, the root-mean-square (r.m.s) fluctuating pressure coefficients C_p' are measured to explore some more details on the differences between vortex lock-on in the lower and higher frequency limits. Figure 19 compares the distributions of C_p' on the front and rear faces for the two lock-on limits with the unforced plate. On the front face, it is found that a fairly flat distribution of C_p' occurs on the unforced plate, but increasing the distance from the rotating axis toward the edges leads to an increase in C_p' for

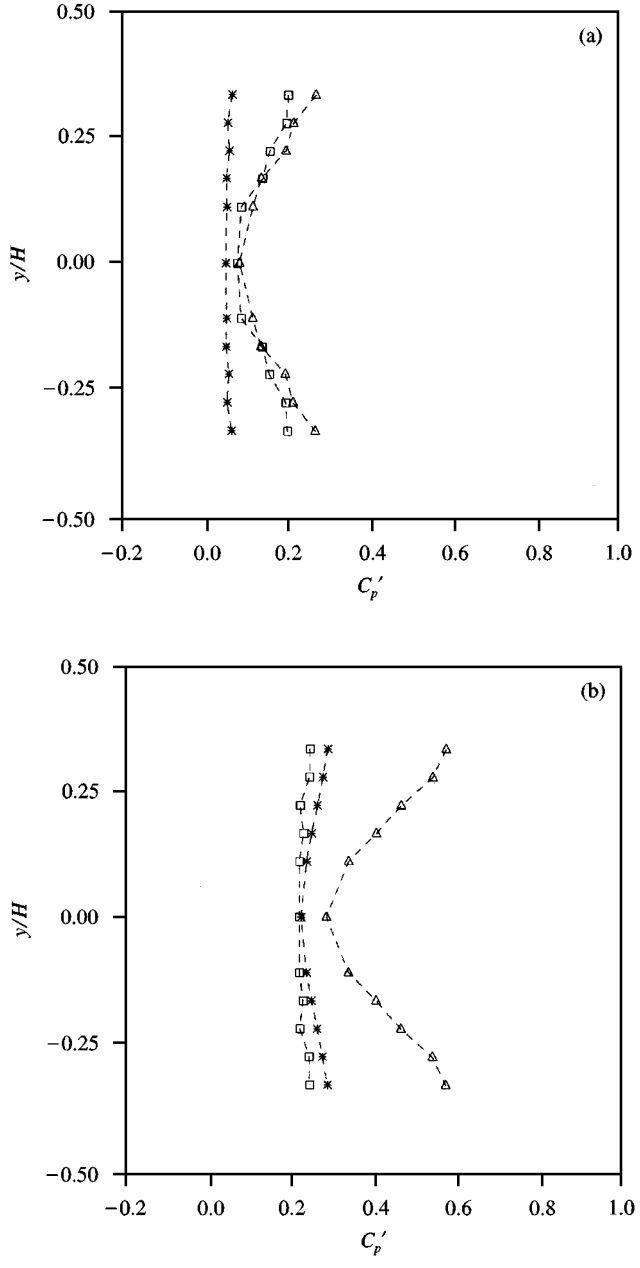

Figure 19. C_p' distributions for: ×, stationary; △, $f_e/f_n = 1{\cdot}047$, $A_0 = 16{\cdot}0°$; □, $f_e/f_n = 0{\cdot}967$, $A_0 = 20{\cdot}0°$ on: (a) the front face; (b) the rear face.

the oscillating plates; in short, the fluctuating pressure seems to vary in accordance with the displacement amplitude of the forcing. On the rear face, the fluctuating pressure for the higher-frequency-limit case is found to increase rapidly with the distance from the middle of the plate, with values much larger than those for the lower-frequency-limit and unforced cases, again signifying the shed vortex developing much closer to the plate as observed in Figure 18. On the other hand, the distribution of C_p' for the lower-frequency-limit case

appears to be even lower than that of the unforced plate, in response to the curvature of the separated shear layer in roll-up portrayed in Figures 15 and 16. The fluctuating pressures presented in Figure 19 also suggest that distribution of C_p' on the rear face is dominated by the structure of the shed vortices rather than by the oscillatory motion of the plate as occurring on the front face.

4. CONCLUSIONS

Experiments have been performed to investigate the lock-on of vortex shedding induced by rotational oscillations of a flat plate which is normal to a uniform stream in its neutral position. The plate was forced to oscillate at a fixed frequency f_e in the neighbourhood of the natural shedding frequency f_n of the stationary normal flat plate for Reynolds numbers based on the plate width in the range of 3000–8000. The onset of lock-on depends on the combination of the frequency and amplitude of the forcing. The route to lock-on as well as the bounds of lock-on regime were examined by using spectral analysis of the wake velocity. Pressure measurements incorporated with flow visualization were carried out to explore the response of the plate to vortex shedding, particularly for the cases in which lock-on occurred.

The state of lock-on can be approached by increasing the amplitude of the forcing from a lower-frequency limit ($f_e < f_n$) or a higher-frequency limit ($f_e > f_n$). As the forcing amplitude is increased, the spectra of the wake velocity demonstrate that the peak amplitude of the vortex-shedding frequency f_v is gradually depressed and that of the forcing frequency is in contrast relatively much enhanced. Once lock-on is reached, the spectrum is dominated by the forcing frequency with a sharp peak. Lock-on can be forced to occur with the least amplitude of the forcing at the natural shedding frequency, i.e. $f_e = f_n$, and the forcing amplitude required for lock-on increases with the difference between f_e and f_n following similar functions of second-order polynomial form for the approach either from the upper or lower limit. The bounds of lock-on regime were found to become narrower with increasing free-stream velocity. It was also found that the only appreciable effect of blockage on the bounds of lock-on regime seems to produce an apparent increase in local free-stream velocity for the range of blockage ratios tested in the current experiments. Nevertheless, further investigation is required for a complete understanding of blockage effects on the vortex lock-on behaviour.

As the lower-frequency limit ($f_e/f_n = 0{\cdot}967$) is approached, the time-mean base pressure distribution appears to be uniform along the plate, with a pressure level slightly higher than that of the unforced plate. This was found to be associated with the formation of a shed vortex, which has a larger curvature in roll-up for the case of lock-on at a lower limit frequency. As the plate is oscillated at a higher limit frequency ($f_e/f_n = 1{\cdot}047$), the base pressure is lower toward the edges of the plate, and the pressure values become more negative with increasing amplitude of the forcing. The appearance of a lower pressure towards the edges is again due to the formation of a shed vortex, which was observed to roll-up closer to the plate and with a larger curvature than those formed behind the plates in the unforced and lower-frequency-limit cases. As compared with the case of an unforced plate, the results of time-mean pressures indicate that the drag coefficient is much increased for lock-on at the higher limit frequency but is slightly reduced at the lower limit frequency. The measurements of the r.m.s. fluctuating pressure on the rear face of the plate also reflect the influence of the formation of shed vortices. When lock-on occurs at the higher limit frequency, the fluctuating base pressure was found to increase rapidly towards the edges, with its values much larger than those on the unforced

plates. As the lower-frequency limit is approached, they are smaller than those on the unforced plate.

ACKNOWLEDGEMENTS

The authors gratefully acknowledge the financial support from the National Science Council of Taiwan, R. O. C. under Contracts NSC 86-2612-E-005-001 and NSC 87-2212-E-005-027.

References

Armstrong, B. J., Barnes, F. H. & Grant, I. 1986 The effect of a perturbation on the flow over a bluff cylinder. *Physics of Fluids* **29,** 2095–2102.

Bearman, P. W. 1984 Vortex shedding from oscillating bluff bodies. *Annual Review of Fluid Mechanics* **16,** 195–222.

Blevins, R. D. 1990 *Flow Induced Vibration*, 2nd edition, Chapter 3. New York: Van Nostrand Reinhold.

Chen, J. M. & Fang, Y. C. 1996 Strouhal numbers of inclined flat plates. *Journal of Wind Engineering and Industrial Aerodynamics* **61,** 99–112.

Chua, K., Lisoski, D., Leonard, A. & Roshko, A. 1990 A numerical and experimental investigation of separated flow past an oscillating flat plate. *International Symposium on Nonsteady Fluid Dynamics* (eds J. A. Miller and D. P. Telionis), FED-Vol. 92, pp. 455–464. New York: ASME.

Fage, A. & Johansen, F. C. 1927 On the flow of air behind an inclined flat plate of infinite span. *Proceedings of the Royal Society* (*London*) **116,** 170–197.

Filler, J. R., Marston, P. L. & Mih, W. C. 1991 Response of the shear layers separating from a circular cylinder to small amplitude rotational oscillations. *Journal of Fluid Mechanics* **231,** 481–499.

Gaster, M. & Ponsford, P. J. 1984 The flow over tapered flat plates normal to the stream. *Aeronautical Journal* **88,** 206–212.

Griffin, O. M. & Ramberg, S. E. 1976 Vortex shedding from a cylinder vibrating in line with an incident uniform flow. *Journal of Fluid Mechanics* **75**, 257–271.

Griffin, O. M. & Hall, M. S. 1991 Review-vortex shedding lock-on and flow control in bluff body wakes. *ASME Journal of Fluids Engineering* **113,** 526–537.

Kelso, R. M., Lim, T. T. & Perry, A. E. 1993 The effect of forcing on the time-averaged structure of the flow past a surface-mounted bluff plate. *Journal of Wind Engineering and Industrial Aerodynamics* **49,** 217–226.

Koopmann, G. H. 1967 The vortex wakes of vibrating cylinders at low Reynolds numbers. *Journal of Fluid Mechanics* **28,** 501–512.

Minewitsch, S., Franke, R. & Rodi, W. 1994 Numerical investigation of laminar vortex-shedding flow past a square cylinder oscillating in line with the mean flow. *Journal of Fluids and Structures* **8,** 787–802.

Nakamura, Y. & Hirata, K. 1991 Pressure fluctuations on oscillating rectangular cylinders with the long side normal to the flow. *Journal of Fluids and Structures* **5,** 165–183.

Novak, J. 1973 Strouhal number and flat plate oscillation in an air stream. *Acta Technica CSAV* **4,** 372–386.

Öngören, A. & Rockwell, D. 1988*a* Flow structure from an oscillating cylinder. Part 1: Mechanisms of phase shift and recovery in the near wake. *Journal of Fluid Mechanics* **191,** 197–223.

Öngören, A. & Rockwell, D. 1988b Flow structure from an oscillating cylinder. Part 2: mode competition in the near wake. *Journal of Fluid Mechanics* **191,** 225–245.

Ota, T., Okamoto, Y. & Yoshikawa, H. 1994 A correction formula for wall effects on unsteady forces of two-dimensional bluff bodies. *ASME Journal of Fluids Engineering* **116,** 414–418.

Pan, D., Chin, Y. C. & Chang, C. H. 1995 Computation of vortex lock-in in the laminar wake of a circular cylinder using unsteady monopole sources. *ASME Journal of Fluids Engineering* **117,** 227–233.

Parkinson, G. V. & Jandali, T. 1970 A wake source model for bluff body potential flow. *Journal of Fluid Mechanics* **40,** 577–594.

ROSHKO, A. 1955 On the wake and drag of bluff bodies. *Journal of Aeronautical Sciences* **22,** 124–132.
SUNG, H. J., KIM, Y. N. & HYUN, J. M. 1994 Discrete vortex simulation of pulsating flow behind a normal plate. *ASME Journal of Fluids Engineering* **116**, 862–869.
STANSBY, P. K. 1976 The locking-on of vortex shedding due to the cross-stream vibration of circular cylinders in uniform and shear flows. *Journal of Fluid Mechanics* **74,** 641–655.
TOKUMARU, P. T. & DIMOTAKIS, P. E. 1991 Rotary oscillation control of a cylinder wake. *Journal of Fluid Mechanics* **224,** 77–90.
YEUNG, W. W. H. & PARKINSON, G. V. 1997 On the steady separated flow around an inclined flat plate, *Journal of Fluid Mechanics* **333,** 403–413.

APPENDIX: NOMENCLATURE

A_0	forcing amplitude
C_D	drag coefficient
C_{Do}	drag coefficient in an unbounded flow
C_p	time-mean pressure coefficient
C_p'	root-mean-square fluctuating pressure coefficient
C_{pb}	time-mean base pressure coefficient
f_e	forcing frequency
f_n	natural vortex shedding frequency of stationary normal flat plate
f_v	vortex-shedding frequency
H	plate width
K	blockage ratio
Re	Reynolds number, $= UH/v$
St	Strouhal number
St_e	forcing Strouhal number, $= f_eH/U$
St_n	natural Strouhal number, $= f_nH/U$
St_o	Strouhal number in an unbounded flow
U	free-stream velocity
U_m	corrected velocity
κ	a parameter in equation (3), $= (1 - C_{pb})^{-1/2}$
ξ	correction factor for blockage

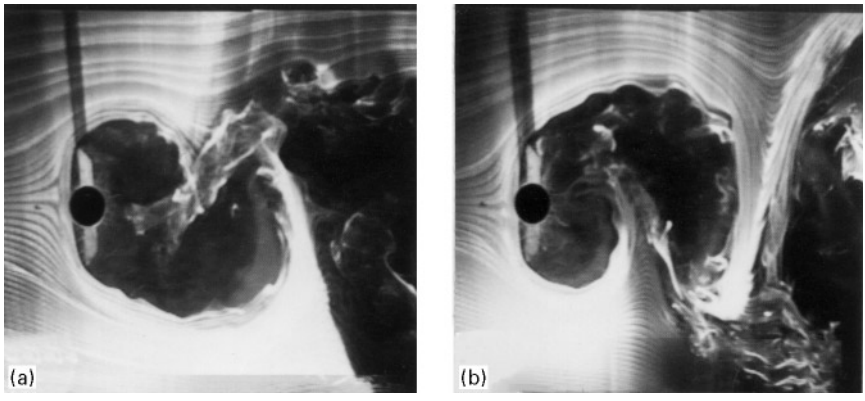

Figure 15. Smoke-wire visualizations for the unforced plate ($H = 45$ mm): (a) vortex shed from the top edge; (b) from the bottom edge.

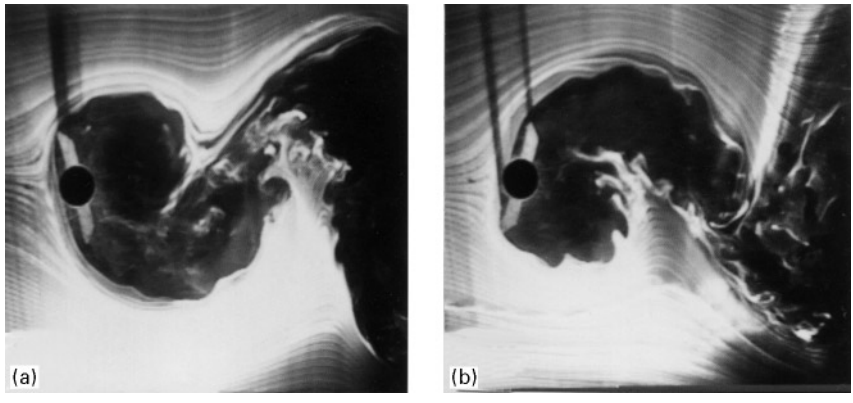

Figure 16. Smoke-wire visualizations for the plate ($H = 45$ mm) oscillated at $f_e/f_n = 0{\cdot}967$, $A_0 = 20{\cdot}0^\circ$: (a) vortex shed from the top edge; (b) from the bottom edge.

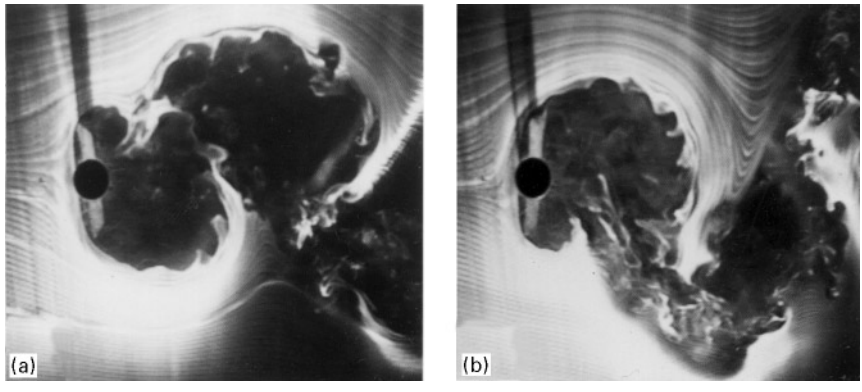

Figure 18. Smoke-wire visualizations for the plate ($H = 45$ mm) oscillated at $f_e/f_n = 1{\cdot}047$, $A_0 = 16{\cdot}0°$: (a) vortex shed from the top edge; (b) from the bottom edge.